Multiple-output microwave single-photon source using superconducting circuits with longitudinal and transverse couplings

Xin Wang, Adam Miranowicz, Hong-Rong Li, and Franco Nori

Phys. Rev. A **94**, 053858 — Published 30 November 2016

DOI: 10.1103/PhysRevA.94.053858

Multi-output microwave single-photon source using superconducting circuits with longitudinal and transverse couplings

Xin Wang,[1,2] Adam Miranowicz,[2,3] Hong-Rong Li,[1] and Franco Nori[2,4]

[1] *Institute of Quantum Optics and Quantum Information, School of Science, Xi'an Jiaotong University, Xi'an 710049, China*

[2] *CEMS, RIKEN, Wako-shi, Saitama 351-0198, Japan*

[3] *Faculty of Physics, Adam Mickiewicz University, 61-614 Poznań, Poland*

[4] *Physics Department, The University of Michigan, Ann Arbor, Michigan 48109-1040, USA*

Single-photon devices at microwave frequencies are important for applications in quantum information processing and communication in the microwave regime. In this work, we describe a proposal of a multi-output single-photon device. We consider two superconducting resonators coupled to a gap-tunable qubit via both its longitudinal and transverse degrees of freedom. Thus, this qubit-resonator coupling differs from the coupling in standard circuit quantum-electrodynamic systems described by the Jaynes-Cummings model. We demonstrate that an effective quadratic coupling between one of the normal modes and the qubit can be induced, and this induced second-order nonlinearity is much larger than that for conventional Kerr-type systems exhibiting photon blockade. Assuming that a coupled normal mode is resonantly driven, we observe that the output fields from the resonators exhibit strong sub-Poissonian photon-number statistics and photon antibunching. Contrary to previous studies on resonant photon blockade, the first-excited state of our device is a pure single-photon Fock state rather than a polariton state, i.e., a highly hybridized qubit-photon state. In addition, it is found that the optical state truncation caused by the strong qubit-induced nonlinearity can lead to an entanglement between the two resonators, even in their steady state under the Markov approximation.

PACS numbers: 42.50.Ar, 42.50.Pq, 85.25.-j

I. INTRODUCTION

In quantum information, the generation, distribution, and storage of quantum information at the single-photon level are of great importance [1–3]. Therefore, single-photon sources of non-classical light states are needed [4, 5]. In some cases, we can reduce the power of a laser or maser source to avoid large probabilities of a multi-photon output. However, the field might be of an extremely low intensity. Photon sources differ not only by their frequencies and polarizations, but also by the statistical properties of the emitted photons [6]. Photons from a coherent source are still classical, while in proposals of security for the quantum cryptography [7] the sources of single-photons exhibiting strong antibunching and sub-Poissonian statistics can help to avoid eavesdropping on an encode message.

To increase the output rate of such sources of non-classical fields, one requires some form of nonlinearity. For example, single-photon manipulation can be realized via photon blockade (see Refs. [8–16] and references therein), in which the nonlinearity prevents more than a single excitation being exited in a cavity: Only when the first photon has left the cavity another identical photon can be reexcited. Photon blockade originates from the anharmonic energy-level structure in nonlinear systems. It has been predicted and demonstrated experimentally in platforms such as optical cavities with a trapped atom [17], integrated photonic crystal cavities with a quantum dot [18, 19], or microwave transmission-line resonators (superconducting "cavities") with a single superconducting artificial atom [20, 21]. Recently, photon blockade and closely related phonon blockade were predicted in optomechanical systems (see, e.g., [22–27]). In the earlier studies, the observation of conventional photon blockade requires large nonlinearities with respect to the decay rate of the system. More recently, it was found that strong entanglement [9, 28] and strong photon antibunching [29, 30] can be generated via destructive quantum interference in coupled nonlinear oscillators: Transition paths for multi-excitations cancel each other and, as a result, the population of the two-photon state is effectively suppressed. This underlying mechanism is called "unconventional photon blockade" and further research has been devoted to it in various kinds of systems [31–36]. It is worth mentioning that the idea of using photon blockade as a single-photon turnstile device was suggested already in the first theoretical works on this effect [9, 11].

The standard single-photon blockade has also been generalized to multiphoton blockade, which is also referred to as photon tunneling. These multiphoton effects have not only been described theoretically (see, e.g., [13, 27, 37–40] and references therein), but even demonstrated experimentally [4, 19, 41–43]. Such multiphoton effects are often discussed in the context of optical state truncation (for a review see Ref. [44, 45]). Here we focus on the standard single-photon blockade, although we also show that multiphoton processes can also be induced in our system.

Recent developments on superconducting quantum devices provide versatile artificial quantum systems for quantum communication and information processing [46–51]. For example, methods for microwave-photon detection based on superconducting quantum circuits have been demonstrated in Refs. [52–56]. Moreover, schemes for measuring photon statistics in the microwave regime have also been proposed both in theoretical and experimental studies [57, 58]. All these progresses have laid a solid foundation for applications at the single-photon level based on superconducting circuits. Therefore, efficient and well-performed single-photon devices in the microwave regime are very important, and have been studied. Resonant photon blockade has been observed in a quantum circuit composed of a superconducting qubit and a transmission-line resonator [21]. Moreover, Ref. [59], discussed the effect of ultrastrong coupling on photon blockade in circuit quantum electrodynamics (QED) systems. All these schemes require the qubit and resonator to be resonant. In another approach [20], the dispersive microwave photon blockade was predicted due to the $\chi^{(3)}$ nonlinearity (about $\sim$1 MHz), which can be induced by a qubit. The sub-Poissonian photon statistics and photon antibunching were also predicted in such systems.

Here we introduce another mechanism to obtain microwave-photon blockade via the effective quadratic coupling in a circuit-QED-based system. Our scheme is composed of two resonators and a single qubit. Different from standard circuit-QED systems with Jaynes-Cummings coupling, our system is based on both longitudinal and transverse couplings. We demonstrate that, in principle, arbitrary multiphoton processes can be induced in our system. In particular, we obtain the effective Hamiltonian for the quadratic coupling between one supermode and the qubit. As opposed to the resonant photon blockade, the first excitation of this system is a bare single-photon state, rather than hybridized with the qubit excited state (i.e., a polariton state), which might provide higher tolerance to imperfections in experiments [20]. The second-order nonlinear coupling strength can be of tens of MHz under current experiment approaches, which is much stronger than the induced $\chi^{(3)}$ nonlinearity in superconducting systems [15, 40]. With a stronger nonlinearity, we can consider resonators with higher-photon escape rates and apply stronger coherent drive fields for the two resonators, and the single-photon output fields can be of much higher intensities. By modeling the quantum input and output fields from channels of independent resonators and joint channels of two resonators, we find that all the three output fields are antibunched and sub-Poissonian in photon-number statistics, so our proposal can serve as an efficient single-microwave photon source with multi-output channels.

The organization of this paper is as follows: In Sec. I, we describe the layout of the model consisting of a qubit and two superconducting resonators, and then we analytically derive the Hamiltonian for multi-photon processes in the two resonators. In Sec. II, we demonstrate how to employ the effective quadratic coupling between the qubit and the resonators to achieve single-photon blockade in the two resonators. After that, we find that it is possible to apply our system as a microwave single photon device with multi-output channels. In Sec. III, we show our numerical results. In particular, we analyze nonclassical photon-number correlations and give a phase-space description of the single-mode (single-resonator) states generated via photon blockade. The last section presents our final discussions and conclusions.

II. MODEL

A. Circuit layout and Hamiltonian

As schematically shown in Fig. 1, we consider a gap-tunable superconducting artificial atom, such as a charge or flux qubit, coupled with two superconducting resonators of frequencies ω_1 and ω_2 [60–63]. Moreover, we assume that the coupling between the resonators is directly mediated via a capacitance C [64]. The Hamiltonian can be written as

$$\begin{aligned}\bar{H}_0 = \frac{1}{2}\omega\bar{\sigma}_z + \frac{1}{2}\Delta\bar{\sigma}_x + \sum_{i=1,2}\omega_i a_i^\dagger a_i \\ +g(a_1^\dagger a_2 + a_2^\dagger a_1) + \bar{\sigma}_z\sum_{i=1,2}G_i(a_i^\dagger + a_i), \quad (1)\end{aligned}$$

where a_i ($a_i^\dagger$) denotes the annihilation (creation) operator for the ith resonator, g is the coupling constant between the two resonators due to the hopping capacitor C, and G_i is the coupling strength between the ith resonator and the qubit. Here we assume that $g \ll G_i$, which justifies the use of the rotating-wave approximation (RWA) in Eq. (1). The Pauli spin operators $\bar{\sigma}_z$ and $\bar{\sigma}_x$ are defined in the basis of the two quantum states of the qubit, and ω and Δ are the energy bias and tunable qubit gap, respectively. In experiments, both ω and Δ can be controlled independently via external parameters. For example, in a flux qubit [65–68], Δ can be tuned by applying an external flux though the superconducting quantum interference loop, while ω can be adjusted by controlling the flux though the qubit loop.

Note that we assume that the inter-resonator coupling g is much smaller than the qubit-resonator couplings G_i. Moreover, these couplings can be strong but not ultrastrong, to justify the application of the RWA. However, the RWA is not valid in the ultrastrong coupling regime, where at least one of the couplings G_i is comparable or larger than the corresponding resonator frequency ω_i. In such a case, due to the counter-rotating terms, photon blockade effects are usually significantly changed compared to the standard blockade under the RWA (see Refs. [59, 69]). For example, Ref. [69] showed that multiple antibunching-to-bunching transitions can be observed when increasing the resonator-qubit coupling strength in the standard (i.e., transverse) Rabi model. These transitions lead to the vanishing and reappearance of pho-

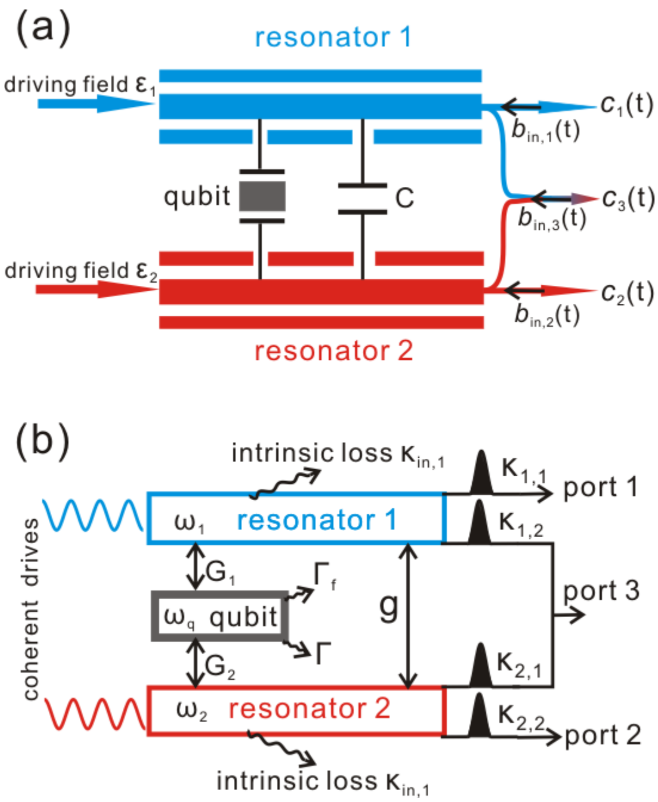

FIG. 1. (Color online) (a) Schematic circuit layout and (b) the couplings and dissipative channels of our proposal. A gap-tunable qubit (e.g., a flux or charge qubit) couples with two superconducting (e.g., transmission-line) resonators with strengths G_i for $i = 1, 2$. The eigenfrequencies for the ith resonator and the qubit are ω_i and ω_q, respectively. A capacitor C is used to directly mediate the two resonators and results in a coupling strength g. In the left-hand side, two coherent microwave drives, with strengths ϵ_1 and ϵ_2, are applied to the resonators 1 and 2, respectively. In the right-hand side, the single photon output microwave photons are collected from ports 1, 2, and 3. Ports 1 and 2 are semi-infinite transmission lines connected to resonators 1 and 2. This results in photon escape rates $\kappa_{1,1}$ and $\kappa_{2,1}$, respectively. Port 3 is the joint output transmission line from resonators 1 and 2, with photon escape rates $\kappa_{1,2}$ and $\kappa_{2,2}$. We assume that the input fields $b_{\text{in},i}$ for these three ports are all independent vacuum noises. Beside escaping into the transmission lines, the photons in the two resonators can also dissipate into the environment with intrinsic rates $\kappa_{\text{in,i}}$. For the qubit, the decay (dephasing) rate is Γ (Γ_f).

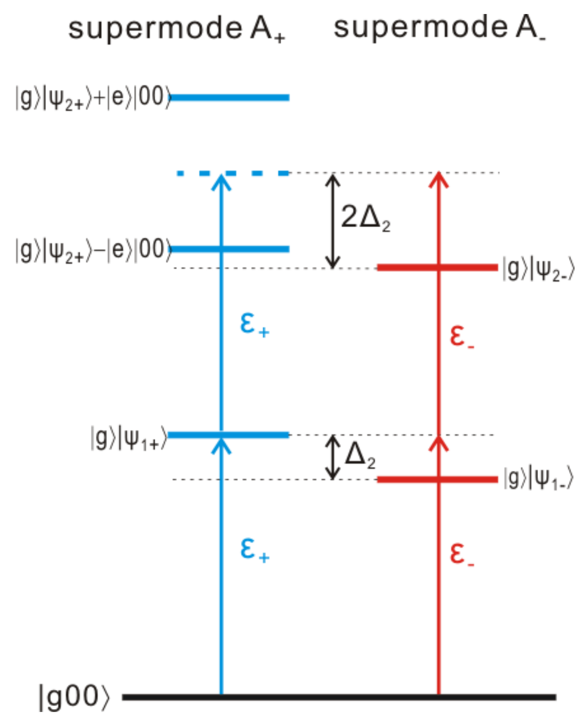

FIG. 2. (Color online) The lowest energy levels for the Hamiltonian in Eq. (14). The supermode A_+ couples with the qubit with quadratic form, while the supermode A_- decouples from the qubit. The frequency difference between these two supermodes is Δ_2. When $\Delta_2 = 0$, these two modes are degenerate. The effective drives for the supermodes A_+ and A_- are ϵ_+ and ϵ_-, respectively, as shown in Table I.

ton blockade due to the presence of the counter-rotating terms, which modify the nonlinearity of the energy spectrum and can cause two-photon cascade decays. We expect that similar effects can be observed in our model if the inter-resonator and qubit-resonator coupling constants are increased.

In the qubit basis, we can write the Hamiltonian in Eq. (1) as

$$H_0 = \frac{1}{2}\omega_q\sigma_z + \sum_{i=1,2}\omega_i a_i^\dagger a_i + g(a_1^\dagger a_2 + a_2^\dagger a_1) + \sum_{i=1,2}\left[G_{x,i}\sigma_x(a_i^\dagger + a_i) + G_{z,i}\sigma_z(a_i^\dagger + a_i)\right], \quad (2)$$

where the coupling constants $G_{x,i} = -G_i \sin\theta$ and $G_{z,i} = G_i \cos\theta$ describe, respectively, the transverse and longitudinal couplings between the qubit and the resonators, with $\tan\theta = \Delta/\omega$, and $\omega_q = \sqrt{\omega^2 + \Delta^2}$ is the transformed qubit eigenfrequency.

In a typical picture of a circuit-QED system, the interaction between cavities and artificial atoms is transverse, which can be simplified to Jaynes-Cummings-type models under the rotating-wave approximation. Another alternative layout for circuit-QED is based on the longitudinal qubit-cavity interaction [70–73]. The Hamiltonian in Eq. (2) describes a qubit with both transverse and longitudinal couplings to the resonators. In such an artificial system, multiphoton Rabi oscillations between a single resonator and a qubit have been predicted in Ref. [63]. In the following discussions, by considering a more general case with two resonators coupled with a qubit, we will analytically obtain the effective Hamiltonians for arbitrary multiphoton processes between the two resonators and the qubit.

We apply two coherent driving fields for the two resonators with strengths ϵ_1 and ϵ_2, respectively, as shown in Fig. 1. Under the rotating-wave approximation, the corresponding driving Hamiltonian is

$$H_d = \sum_{i=1,2} (\epsilon_i a_i^\dagger e^{-i\omega_{d,i}t} + \epsilon_i^* a_i e^{i\omega_{d,i}t}), \tag{3}$$

and the total Hamiltonian for the system can be expressed as

$$H_s = H_0 + H_d. \tag{4}$$

The two driving fields might have a phase difference θ. By assuming that $\epsilon_1 = |\epsilon_1|e^{-i\theta/2}$ and $\epsilon_2 = |\epsilon_2|e^{i\theta/2}$, we will in Sec. IV.B show that both the relative phase θ and the drive strength $|\epsilon_i|$ have significant effects on the photon distribution statistics of the output fields.

B. Multiphoton processes

To explicitly demonstrate multiphoton processes between the qubit and the two resonators, we first introduce the two supermodes via their annihilation operators:

$$A_+ = \frac{G_1 a_1 + G_2 a_2}{\overline{G}}, \tag{5a}$$

$$A_- = \frac{G_2 a_1 - G_1 a_2}{\overline{G}}, \tag{5b}$$

where $\overline{G} = \sqrt{G_1^2 + G_2^2} = G_1\sqrt{1+\beta^2}$, and the commutation relation between A_i and $A_j^\dagger$ is $[A_i, A_j^\dagger] = \delta_{ij}$. We define $\beta = G_1/G_2$ as the ratio of the coupling strengths. The detuning between the resonator fundamental frequencies should satisfy the relation

$$\omega_1 - \omega_2 = g(\beta^2 - 1)/\beta. \tag{6}$$

Assuming that the two drives are of the same frequency $\omega_{d,i} = \omega_d$, we express H_s in Eq. (4) in terms of A_+ and A_- as follows:

$$H_s = \frac{1}{2}\omega_q\sigma_z + \sum_{i=\pm}\Omega_i A_i^\dagger A_i + G_z\sigma_z(A_+^\dagger + A_+) + G_x\sigma_x(A_+^\dagger + A_+) + \sum_{i=\pm}\epsilon_i(A_i^\dagger e^{-i\omega_d t} + \text{H.c.}), \tag{7}$$

where the renormalized eigenfrequencies $\Omega_\pm$ and the driving strengths $\epsilon_\pm$ for the supermodes $A_\pm$ are presented in Table I, and

$$G_z = \overline{G}\cos\theta, \tag{8a}$$

$$G_x = -\overline{G}\sin\theta \tag{8b}$$

are the longitudinal and transverse coupling strengths between the qubit and the supermode A_+, respectively. From Eq. (7), we find that the supermode A_- decouples from the qubit. Let us apply the frame rotated by the unitary polariton transformation $\exp[-\lambda\sigma_z(A_+^\dagger - A_+)]$, with $\lambda = G_z/\Omega_+$ [62, 74], and use the commutation relation

$$[A_+, f(A_+, A_+^\dagger)] = \frac{\partial f(A_+, A_+^\dagger)}{\partial A_+},$$

where $f(A_+, A_+^\dagger)$ can be expanded in a power series of the supermodes A_+ and $A_+^\dagger$. Then the total Hamiltonian becomes

$$H_s = \frac{1}{2}\omega_q\sigma_z + \sum_{i=\pm}\Omega_i A_i^\dagger A_i + G_x\left\{\sigma_+\left[A_+^\dagger f(\lambda) + f(\lambda)A_+\right] + \text{H.c.}\right\} + \sum_{i=\pm}\epsilon_i(A_i^\dagger e^{-i\omega_d t} + \text{H.c.}) - 2\lambda\epsilon_+\sigma_z\cos(\omega_d t), \tag{9}$$

where $f(\lambda) = \exp[2\lambda(A_+^\dagger - A_+)]$. For weak driving strengths $\epsilon_{1,2}$ and a small Lamb-Dicke parameter $\lambda \ll 1$ [75], $2\lambda\epsilon_+$ is a much smaller parameter. Therefore the last term in $\tilde{H}_s$ can be neglected.

Let us now show how to realize multi-photon processes by setting $\omega_q \simeq n\Omega_+$, with n being the order of the photon-qubit transitions. By expanding the third terms in Eq. (9) in terms of the small parameter λ, and keeping only the resonant terms, we obtain the corresponding Hamiltonian for the n-photon processes,

$$\begin{aligned} H_n &= G_x \textstyle\sum_{m=1}^{\infty}\left[B_1(m,n)\sigma_+ A_+^{\dagger m} A_+^{m+n} + \text{H.c.}\right] \\ &+ G_x \textstyle\sum_{m=0}^{\infty}\left[B_2(m,n)\sigma_+ A_+^{\dagger m} A_+^{m+n} + \text{H.c.}\right], \end{aligned} \tag{10}$$

	Supermode A_+	Supermode A_-
Eigenfrequencies	$\Omega_+ = \omega_1 + \frac{g}{\beta}$, $\Omega_+^{'} = \Omega_+ - \frac{4G_x^2}{3\Omega_+}$	$\Omega_- = \omega_2 - \frac{g}{\beta}$
Driving strengths	$\epsilon_+ = \frac{\beta\epsilon_1+\epsilon_2}{\sqrt{1+\beta^2}}$	$\epsilon_- = \frac{\epsilon_1-\beta\epsilon_2}{\sqrt{1+\beta^2}}$
First-excited states	$\|\psi_{1+}\rangle = \frac{\beta\|10\rangle+\|01\rangle}{\sqrt{1+\beta^2}}$	$\|\psi_{1-}\rangle = \frac{\|10\rangle-\beta\|01\rangle}{\sqrt{1+\beta^2}}$
Second-excited states	$\|\psi_{2+}\rangle = \frac{\beta^2\|20\rangle+\sqrt{2}\beta\|11\rangle+\|02\rangle}{1+\beta^2}$	$\|\psi_{2-}\rangle = \frac{\|20\rangle-\sqrt{2}\beta\|11\rangle+\beta^2\|02\rangle}{1+\beta^2}$
Effective nonlinear coupling	couples with the qubit	decouples from the qubit

TABLE I. The parameters and eigenstates of the two supermodes A_+ and A_-, according to the Hamiltonian in Eq. (14).

where the coefficients $B_i(m,n)$ are expressed as

$$B_1(m,n) = e^{-2\lambda^2}\frac{(-1)^{m+n}(2\lambda)^{2m+n-1}}{(m-1)!(m+n)!}, \tag{11a}$$

$$B_2(m,n) = e^{-2\lambda^2}\frac{(-1)^{m+n-1}(2\lambda)^{2m+n-1}}{m!(m+n-1)!}. \tag{11b}$$

From Eq. (10), we conclude that, in principle, arbitrary multi-photon processes between the qubit and one supermode of the two resonators can be induced in this circuit-QED system. However, for a small parameter λ, the rates of n-photon transitions, which are determined by $B_1(m,n)$ and $B_2(m,n)$, decrease rapidly with increasing m and n; so higher-order photon-qubit transitions have slower rates and, therefore, can be overwhelmed by the rapid oscillation terms and decoherence channels.

In experiments, the interaction in a circuit-QED system can easily enter into the strong-coupling regime [76–78]. For two superconducting resonators oscillating at frequency $\omega_i/(2\pi)$=2.5 GHz with G_i=0.06ω_i, and by setting $\theta = \pi/4$, the rates for the two-photon ($n = 2$) and three-photon transitions ($n = 3$) between the qubit and the supermode A_+ are $\Theta_2/(2\pi) \simeq$18 MHz and $\Theta_3/(2\pi) \simeq$1.1 MHz, respectively.

Here we assume that the qubit should be operated around its optimal point (but not exactly at this point), so the dephasing noise of the qubit is the dominant decoherence channel. As reported in Ref. [79], for a flux qubit operated around the optimal point (the flux bias is $\Phi_b \sim 1\times10^{-3}\Phi_0$, with Φ_0 being the flux quantum), the dephasing rate was measured about 6 μs^{-1} (the corresponding dephasing rate $\Gamma_f/(2\pi) \simeq 1$ MHz). The quality factor Q of a superconducting resonator can easily exceed 10^4 [80] (i.e., the decay rate $\gamma/(2\pi) \simeq$0.25 MHz). Thus, the rate for the two-photon (three-photon) transitions exceeds (is comparable to) all the decoherence rates in current experimental implementations, and it is possible to observe quantum coherent phenomena due to these multiphoton processes.

III. ANALYTICAL RESULTS

A. Photon blockade in two resonators

In this part, we will demonstrate the single-photon blockade in the two resonators, which can be induced by the two-photon processes. By setting $\omega_q \simeq 2\Omega_+ \gg G_x$ and neglecting the last term, we expand Eq. (9) to first order in λ, and obtain

$$H_s \cong \frac{1}{2}\omega_q\sigma_z + \sum_{i=\pm}\Omega_i A_i^\dagger A_i + G_x\sigma_x(A_+^\dagger + A_+) + 2\lambda G_x\left[\sigma_+(A_+^{\dagger 2} - A_+^2) + \text{H.c.}\right] + \sum_{i=\pm}\epsilon_i(A_i^\dagger e^{-i\omega_d t} + \text{H.c.}). \tag{12}$$

The effective Hamiltonian for the third term can be expressed as $4G_x^2/(3\Omega_+)\,\sigma_z A_+^\dagger A_+$, which can be viewed as the dispersive coupling between the qubit and the supermode A_+ [81]. In this paper, we find that the qubit remains effectively in its ground state, so this term will only renormalize the eigenfrequency of the supermode A_+ to $\Omega_+^{'} = \Omega_+ - 4G_x^2/(3\Omega_+)$. Assuming $\omega_q = 2\Omega_+^{'}$, and performing the unitary transformation

$$U = \exp\left\{-i\omega_d\sigma_z t - i\sum_{i=\pm}\omega_d A_i^\dagger A_i t\right\}, \tag{13}$$

we obtain the following time-independent Hamiltonian by neglecting the fast-oscillating terms in H_s

$$H_{\rm eff} = \frac{1}{2}\Delta_+\sigma_z + \sum_{i=\pm}\Delta_i A_i^\dagger A_i + \Theta\left(\sigma_+ A_+^2 + \sigma_- A_+^{\dagger 2}\right) + \sum_{i=\pm}\epsilon_i(A_i^\dagger + A_i), \quad (14)$$

where $\Theta = -2\lambda G_x$, $\Delta_+ = \Omega_+^{'} - \omega_d$ is the frequency detuning between the supermode A_+ and the drive field, and $\Delta_- = \Delta_+ + \Delta_2$ with

$$\Delta_2 = \frac{4G_x^2}{3\Omega_+} - \frac{g(1+\beta^2)}{\beta} \quad (15)$$

is the frequency difference between these two supermodes, which can be obtained from the parameters in Eq. (6) and Table I. The third term in Eq. (14) describes the quadratic coupling between the supermode A_+ and the qubit, while the supermode A_- decouples from the qubit. Moreover, the supermode A_+ (A_-) is driven with strength ϵ_+ (ϵ_-) and detuning Δ_+ (Δ_-).

As shown in Table I, the ground state of the system is $|g\rangle \otimes |\psi_0\rangle = |g\rangle|00\rangle$, and the first-excited states for the supermodes A_+ and A_- are the single-photon entangled states

$$|\psi_{1\pm}\rangle = \frac{G_1|10\rangle \pm G_2|01\rangle}{\sqrt{G_1^2+G_2^2}}. \quad (16)$$

Without the nonlinear coupling of the resonators with the qubit, the second-excited states for the supermodes A_+ and A_- become $|\psi_{2+}\rangle$ and $|\psi_{2-}\rangle$, respectively, which are defined by

$$|\psi_{2\pm}\rangle = \frac{G_1^2|10\rangle \pm G_1G_2|10\rangle + G_2^2|01\rangle}{G_1^2+G_2^2}. \quad (17)$$

However, due to the effective nonlinear coupling, the second excited states for supermode A_+ are the two dressed (as marked by the subscript d) states

$$|\Psi_{d,\pm}\rangle = \frac{|g\rangle|\psi_{2+}\rangle \pm |e\rangle|00\rangle}{\sqrt{2}} \quad (18)$$

with energy splitting $2\sqrt{2}\Theta$, as shown in Fig. 2. As a consequence, the energy levels of supermode A_+ become anharmonic. It should be noted that $\epsilon_\pm$ can conveniently be adjusted by changing the pumping strengths ϵ_1 and ϵ_2, as presented in Table I. Hence, under the conditions: $\Delta_- \gg \epsilon_-$, or $\epsilon_- \simeq 0$, the supermode A_- cannot be driven effectively. Meanwhile, if the supermode A_+ are resonantly driven with strength ϵ_+, the state $|\psi_{1+}\rangle$ will be occupied, and the first photon can enter into the two resonators. However, the two-photon state $|\psi_{2+}\rangle$ can hardly be excited due to the non-existence of available states. Thus, for the two resonators, the two-photon states $|20\rangle$, $|02\rangle$, and $|11\rangle$ will be of extremely low probabilities. Similar to the case in Refs. [28, 82], the Hilbert space of this composite system is only spanned by the vacuum and single-photon states. These two resonators behave as a qubit with the ground and excited states being $|\psi_0\rangle = |00\rangle$ and $|\psi_{1+}\rangle$, respectively.

B. Input-output relations for the three ports

We consider the input and output ports as sketched in Fig. 1. At the outer edges, each resonator is capacitively coupled to two semi-infinite transmission lines [64]. By combining one transmission line of each resonator as port 3 [83], we achieve three input and output ports. Here we discuss the first-order correlation features of the output field from these three channels. The second-order correlation functions will be discussed in Sec. IV.C.

The corresponding boson operators for the input and output modes of the ith port are denoted as $b_{{\rm in},i}$ and c_i, respectively. According to the input-output relations, the input, output, and intra-resonator fields are linked through the boundary conditions [83–85],

$$c_1 = b_{{\rm in},1} + \sqrt{\kappa_{1,1}}a_1, \quad (19a)$$
$$c_2 = b_{{\rm in},2} + \sqrt{\kappa_{2,1}}a_2, \quad (19b)$$
$$c_3 = b_{{\rm in},3} + \sqrt{\kappa_{1,2}}a_1 + \sqrt{\kappa_{2.2}}a_2, \quad (19c)$$

where $\kappa_{i,j}$ is the photon escape rate from the resonator i to its jth line [64, 83]. With the intrinsic loss rate $\kappa_{{\rm in},i}$ of the resonator i, the total loss rate for this resonator can be expressed as $\gamma_i = \kappa_{{\rm in},i} + \kappa_{i,1} + \kappa_{i,2}$. Without loss of generality, we assume that the decay rates of all the channels for each resonator are the same, i.e., $\kappa_{{\rm in},i} = \kappa_{i,j} = \frac{\gamma_i}{3}$ for $i,j = 1,2$. Moreover, the input fields $b_{{\rm in},i}$ of the three ports are all independent quantum vacuum noises, and satisfy the Markov correlation relations:

$$\langle b_{{\rm in},i}(t)b_{{\rm in},j}^\dagger(t^{'})\rangle = \delta(t-t^{'})\delta_{ij}, \quad (20)$$

so all the normally-ordered cross correlations between the intra-resonator and input field are zero, and the correlations of output fields at each port can be expressed only with the resonator operators. The average output photon numbers collected through the three ports, which are proportional to the first-order correlation functions with the zero-time delay, can be expressed as

$$N_1 = \langle c_1^\dagger c_1\rangle = \frac{\gamma_1}{3}\langle a_1^\dagger a_1\rangle, \quad (21a)$$
$$N_2 = \langle c_2^\dagger c_2\rangle = \frac{\gamma_2}{3}\langle a_2^\dagger a_2\rangle, \quad (21b)$$
$$N_3 = \langle c_3^\dagger c_3\rangle = \frac{\gamma_1\langle a_1^\dagger a_1\rangle + \gamma_2\langle a_2^\dagger a_2\rangle}{3} + \frac{\sqrt{\gamma_1\gamma_2}(\langle a_1^\dagger a_2\rangle + \langle a_2^\dagger a_1\rangle)}{3}. \quad (21c)$$

We will apply these input-output relations, in particular, in Sec. IV.C.

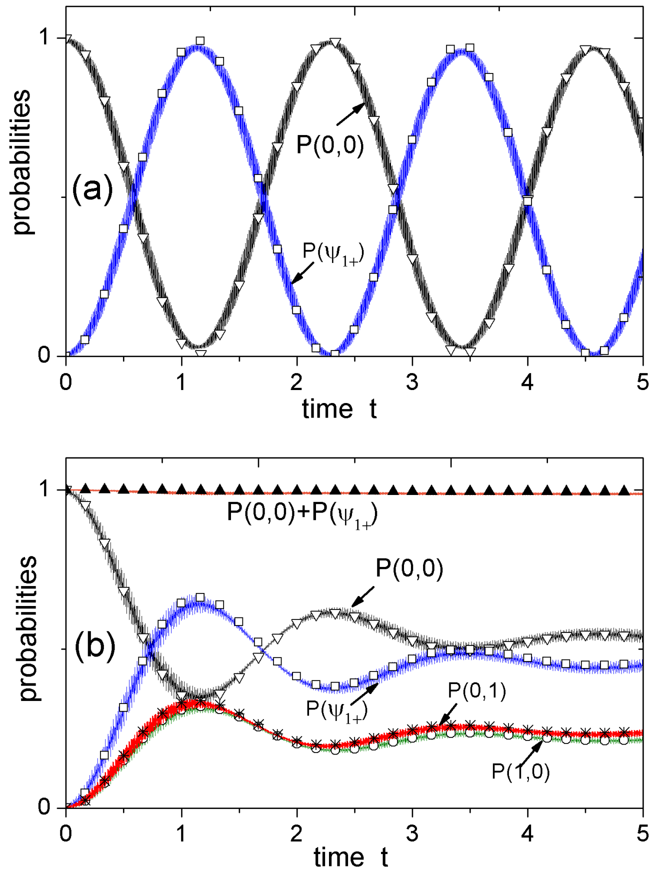

FIG. 3. (Color online) Time evolutions of the probabilities for the system described by $H = H_s$ (shown with solid curves) and $H = H_{\rm eff}$ (marked with symbols) in the (a) nondissipative and (b) dissipative cases. The initial state is $|0,0\rangle|g\rangle$. (a) Without considering any decay channels, the time-evolution of the probabilities $P(0,0)$ and $P(\psi_{1+})$ exhibit the Rabi oscillations between the states $|0,0\rangle$ and $P(\psi_{1+})$. (b) The decay of the probabilities assuming the decoherent rates $\Gamma = \Gamma_f/2 = \gamma_1 = \gamma_2 = 1$. We find that the sum of $P(0,0)$ and $P(\psi_{1+})$ is almost equal to 1 for all the evolution times. Thus, this sum can be considered as a fidelity measure of optical state truncation resulting in photon blockade. Here we consider that the two modes are degenerate, i.e., $\Delta_2 = 0$.

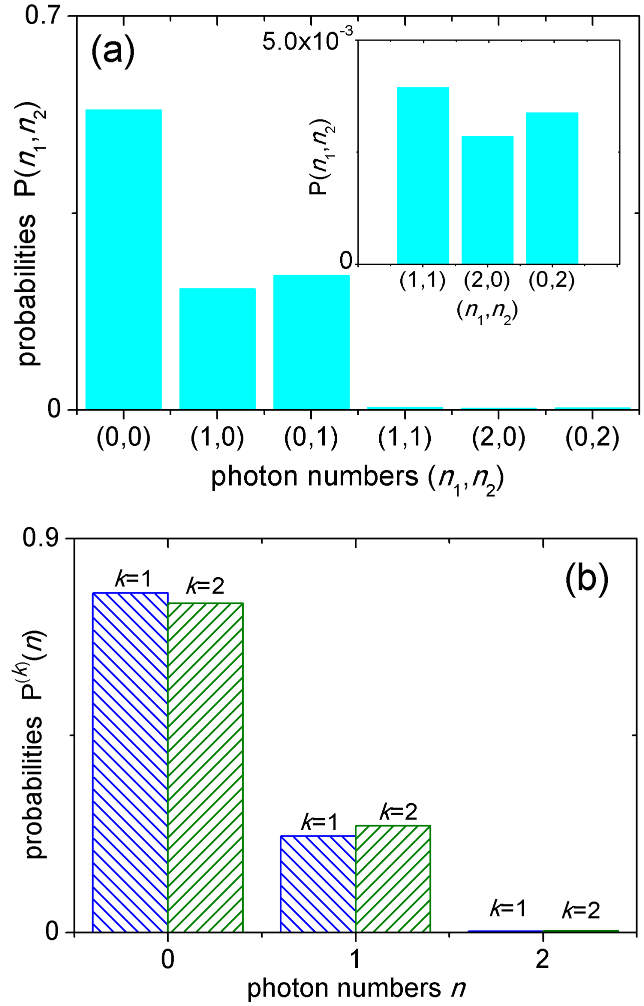

FIG. 4. (Color online) (a) Two-resonator photon-number probabilities $P(n_1, n_2)$ and (b) photon-number probabilities $P^{(k)}$ of the resonator $k = 1$ and $k = 2$ for the output steady state (i.e., for $t \to \infty$) for the same parameters as those in Fig. 3(b). It can be found that the multi-photon states are hardly excited.

IV. NUMERICAL RESULTS

A. Time-dependent solutions of the master equation

In this section, we numerically demonstrate that single-photon blockade can occur in our system even assuming amplitude and phase damping as described by the master equation. Numerical computations of the time-evolution solution of the master equation were performed using the Python package QuTiP [86, 87].

With Γ_f (Γ) denoting the pure dephasing (decay) rate of the qubit, the evolution of the reduced density operator $\rho(t)$ is governed by the standard Lindblad-Kossakowski master equation,

$$\frac{d\rho(t)}{dt} = -i[H, \rho(t)] + \Gamma D[\sigma_-]\rho(t) + \frac{\Gamma_f}{2} D[\sigma_z]\rho(t) + \sum_{i=1,2} \gamma_i D[a_i]\rho(t), \quad (22)$$

where the Lindblad superoperator D, acting on $\rho(t)$ with a given collapse operator B, is defined by $D[B]\rho = B\rho B^\dagger - \frac{1}{2}(B^\dagger B\rho - \rho B^\dagger B)$. For simplicity, we assume that all the parameters are dimensionless. By setting $\beta = 1$, we choose the two resonators with the same frequency $\omega_i = 2500$ and the same coupling strength $G_i = 0.06\omega_i$. As a result, the effective quadratic coupling strength is $\Theta = 18$. We applied two coherent drives with the unbalanced strengths $\epsilon_1 = 0.95$ and $\epsilon_2 = 1$ for the two resonators. As a result, the two supermodes A_+ and A_-

are driven resonantly with the strengths $\epsilon_+ = 1.38$ and $\epsilon_- = -0.035$, respectively (which can be calculated via the relations shown in Table I).

First, we consider the two supermodes are degenerate, i.e., $\Delta_2 = 0$. According to Eq. (15) we obtain the direct coupling strength between the two resonators to be equal to $g = 6$. Defining the probabilities

$$\begin{aligned} P(n_1, n_2) &= \langle n_1, n_2|\rho(t)|n_1, n_2\rangle, \\ P^{(k)}(n) &= \langle n_k|\rho(t)|n_k\rangle, \\ P(\psi_{1+}) &= \langle \psi_{1+}|\rho(t)|\psi_{1+}\rangle \end{aligned}$$

for the Fock states $|n_1, n_2\rangle$, $|n_k\rangle$ (the Fock states of the kth resonator), and the Bell-state $|\psi_{1+}\rangle$, we numerically simulate the original Hamiltonian $H = H_s$ in Eq. (4) and the effective Hamiltonian $H = H_{\rm eff}$ in Eq. (14), respectively. The time-dependent evolutions are plotted in Fig. 3, where subplot (a) [(b)] corresponds to the nondissipative (dissipative) case.

It can be seen that the dynamical evolutions governed by $H_{\rm eff}$ (the curves marked with symbols) and H_s (the solid oscillating curves) match well each other in both nondissipative and dissipative cases, indicating that the approximations adopted for deriving the effective Hamiltonian are valid. Since $\Theta \gg \epsilon_+$ and $\gamma_{1,2} \gg \epsilon_-$, only the first excited state $|\psi_{1+}\rangle$ of the supermode A_+ can be excited effectively. Therefore, the Hilbert space of two resonators is truncated into a two-level system due the quadratic coupling. In Fig. 3(a), we find that the amplitudes of $P(0, 0)$ and $P(\psi_{1+})$ approximately exhibit qubit-like Rabi oscillations without the consideration of any decay channel.

In Fig. 3(b), we consider the dissipative case, and find that the sum of $P(0, 0)$ and $P(\psi_{1+})$ is almost equal to 1, so the multiphoton probabilities $P(n_1, n_2)$ with $n_1 + n_2 \geq 2$ are of extremely low amplitudes. In this case, the two resonators behave as a single qubit. In Fig. 4, we plot the probabilities for photon states (n_1, n_2) and the photon number distribution of each resonator for the original Hamiltonian $H = H_s$ when $t \to \infty$. We find that, for each resonator, only a single-photon state can be excited. For the two resonators, the probabilities of multi-photon states are all smaller than 5×10^{-3}, while the states $P(0, 0)$, $P(0, 1)$, and $P(1, 0)$ are effectively occupied. This phenomenon can be explained as single-photon two-resonator blockade; that is, only one photon can be detected in these two resonators during two zero-time-delay measurements.

Note that we describe the dissipative dynamics of our system by the standard master equation under the Markov approximation and assume weak couplings among all subsystems: the qubit, each resonator, and the environment. To capture the non-Markovian effects on the photon blockade, one can use, e.g., the effective Keldysh action formalism [88], as recently applied in a similar physical context in Ref. [89]. Moreover, to study photon blockade in our system in the ultrastrong or deep-strong coupling regimes, the generalized master equation can be applied within the general formalism of Breuer and Petruccione (see sect. 3.3 in Ref. [90]). This generalized master equation was derived in detail for a circuit-QED system in Ref. [91]. In that approach all subsystems (in our case: the qubit and two resonators) would dissipate into a single entangled channel. This is in contrast to the standard master equation, as analyzed here, where we assume separable dissipation channels for each subsystem.

In the following sections, we focus on the steady-state solutions of the master equation, i.e., $\rho_{\rm ss} \equiv \lim_{t\to\infty} \rho(t)$, by adopting the time-independent Hamiltonian $H = H_{\rm eff}$ and using a shifted inverse power method implemented in Ref. [87].

B. Phase-space description of photon blockade

To visualize the nonclassical properties of the fields generated in our superconducting circuit, we apply the phase-space formalism of Cahill and Glauber [92]. This formalism enables a complete description of the dynamics of any quantum system in terms of quasiprobability distributions (QPDs) and, thus, without applying operators and their corresponding calculus (as in the standard quantum-mechanical formalisms of, e.g., Schrödinger and Heisenberg).

The Cahill-Glauber s-parametrized QPD, $\mathcal{W}^{(s)}(\alpha)$, for $s \in [-1, 1]$, of a given single-mode state ρ can be defined via its Fock state representation as follows [92]:

$$W^{(s)}(\alpha) = \sum_{k,l=0}^{\infty} \langle k|\rho|l\rangle\langle l|T^{(s)}(\alpha)|k\rangle, \tag{23}$$

given in terms of the operator $T^{(s)}(\alpha)$, which can be defined via its Fock-state elements:

$$\langle l|T^{(s)}(\alpha)|k\rangle = c\sqrt{\frac{l!}{k!}}\, y^{k-l+1} z^l (\alpha^*)^{k-l} L_l^{k-l}(x_\alpha), \tag{24}$$

where $x_\alpha = 4|\alpha|^2/(1-s^2)$, $y = 2/(1-s)$, $z = (s+1)/(s-1)$, $c = (1/\pi)\exp[-2|\alpha|^2/(1-s)]$, and L_l^{k-l} are the associated Laguerre polynomials [93]. The real and imaginary parts of the QPD argument α are usually identified as the canonical position and momentum, respectively. It is seen that this s-parametrized QPD is a generalization of the Wigner W function for $s = 0$, the Husimi Q function for $s = -1$, and the Glauber-Sudarshan P function in the limiting case for $s = 1$.

The generalization of these single-mode QPDs for the multimode case is straightforward. However, for brevity, we will not present this generalization here, but will focus on the QPDs given by Eq. (23) for the single-mode (i.e., first-resonator) reduced output states.

In Fig. 5 we plotted the s-parametrized QPDs for (a) $s = 0$ (which corresponds to the Wigner function), (b) $s = 1/2$ and (c) $s = 0.54$ for a given choice of parameters of our system. These plots are tomographic projections

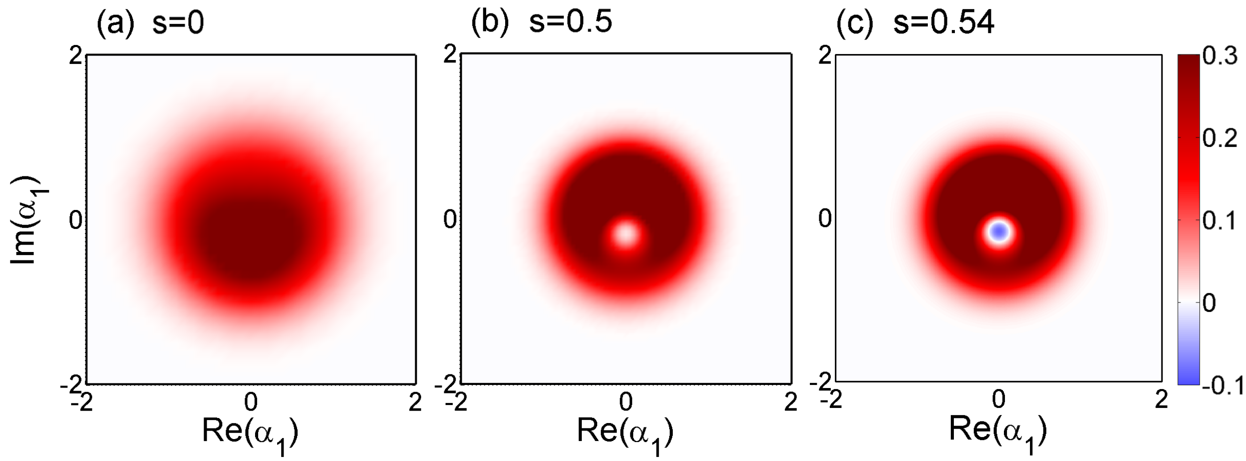

FIG. 5. (Color online) Single-resonator quasiprobability distributions $W^{(s)}$ with parameter (a) $s=0$ (corresponding to the Wigner function), (b) $s=1/2$, and (c) $s=0.54$ for the steady-state solutions $\rho_{\rm ss}^{(1)}={\rm Tr}_2(\rho_{\rm ss})$ of the first resonator as a function of its canonical position ${\rm Re}(\alpha_1)$ and momentum ${\rm Im}(\alpha_1)$. The corresponding plots for the second resonator for $\rho_{\rm ss}^{(2)}={\rm Tr}_1(\rho_{\rm ss})$ are very similar to these and, thus, are not presented here. The other parameters used here are the same as those in Fig. 3(b). The negativity of the QPD shown in panel (c) clearly reveals the nonclassical character of the state generated via photon blockade. We note that the parameter $s=0.54$ was chosen to be slightly larger than the nonclassical depth $s_0=0.537$ of the state (or more precisely, of the corresponding perfectly-truncated qubit state). Thus, the QPD shown in (c) is non-positive, as indicated by the blue region.

of the QPDs, where their negative regions are marked in blue, as seen in Fig. 5(c) for some values of the canonical position ${\rm Re}(\alpha_1)$ and momentum ${\rm Im}(\alpha_1)$ of the first resonator. The negative regions of a given QPD reveal the nonclassical character of the generated state. For a precise definition of nonclassicality as well as its measures and witnesses see, e.g., Refs. [94, 95] and references therein. It is seen that only the QPD shown in Fig. 5(c) explicitly shows the nonclassicality of the analyzed state. This nonclassicality cannot be easily concluded by analyzing, e.g., the nonnegative Wigner function in Fig. 5(a).

The Cahill-Glauber formalism enables to define measures of nonclassicality (or quantumness) of a quantum system. These include the nonclassical depth τ [96] (for a recent review see Ref. [95]). This measure can be defined as the minimum amount of Gaussian noise (quantified by the parameter s) required to destroy the nonclassicality or, equivalently, to change the negative function $P\equiv\mathcal{W}^{(1)}$ into a non-negative $\mathcal{W}^{(s_0)}$, i.e.:

$$\mathcal{W}^{(s_0)}(\alpha)=\min_s c'\int\exp\left(-\frac{2|\alpha-\beta|^2}{1-s}\right)\mathcal{W}^{(1)}(\beta){\rm d}^2\beta\geq 0, \tag{25}$$

where $s_0,s\in[-1,1)$ and $c'=2/[\pi(1-s)]$. The Lee nonclassical depth τ for a given state ρ corresponds to this minimal Cahill-Glauber parameter s_0 as follows

$$\tau(\rho)=\frac{1}{2}(1-s_0). \tag{26}$$

Recently, it was shown that the nonclassical depth for a qubit state, defined by the vacuum and single-photon states, is given by [95]:

$$\tau(\rho)=\frac{\langle 1|\rho|1\rangle^2}{\langle 1|\rho|1\rangle-|\langle 0|\rho|1\rangle|^2}. \tag{27}$$

Thus, if a perfect qubit state could be generated by photon blockade, then its nonclassicality can be exactly given by Eq. (27). However, in our system we predicted the generation of only effective non-perfect qubit states, which have a minor contribution from the Fock states with a larger number of photons. Specifically, the contribution of such terms is less than 5×10^{-3}, as seen in the subset of Fig. 4(a). Such imperfections of an effective qubit state result in its nonclassical depth to be only approximately given by Eq. (27).

For the system parameters chosen in Fig. 5, the nonclassical depth is $\tau(\bar\rho_{\rm ss}^{(1)})=0.23$, which corresponds to $s_0=0.537$, where $\bar\rho_{\rm ss}^{(1)}$ is the single-resonator generated state $\rho_{\rm ss}^{(1)}={\rm Tr}_2(\rho_{\rm ss})$, which is artificially truncated to the qubit Hilbert space. The nonclassical depth for the state $\rho_{\rm ss}^{(1)}$, which is calculated numerically with a high precision in a higher-dimensional Hilbert space, is only slightly larger than that obtained for the qubit truncated state $\bar\rho_{\rm ss}^{(1)}$.

C. Nonclassical photon-number correlations in photon blockade

Here we analyze nonclassical photon-number correlations of the stationary output fields generated in our superconducting system. We will show that the output signals in all the three ports can exhibit both sub-Poissonian

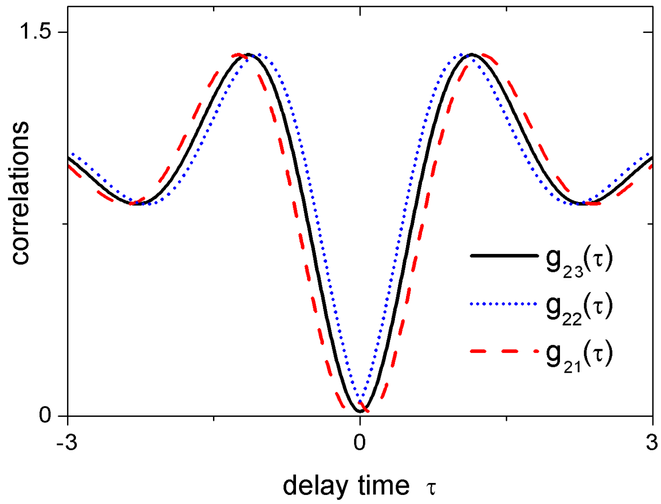

FIG. 6. (Color online) The two-time second-order correlation functions $g_{21}(\tau)$ (red dashed curve), $g_{22}(\tau)$ (blue dot curve) and $g_{23}(\tau)$ (black solid curve) as functions of the delay time τ for ports 1, 2 and 3. All these three second-order correlation functions are much smaller than 1, and show dips at zero-time delay $\tau = 0$. These dips reveal strong sub-Poissonian photon number statistics, since $g_{2i}(\tau = 0) \approx 0$, while the increase of $g_{2i}(\tau)$ with increasing τ from $\tau = 0$ reveal photon antibunching. The parameters used here are the same as those in Fig. 3(b).

photon-number statistics and photon antibunching under appropriate conditions.

Let us define the time-delay second-order correlation function of the output field of the steady state as

$$g_{2i}(\tau) = \lim_{t\to\infty} \frac{\langle c_i^\dagger(t) c_i^\dagger(t+\tau) c_i(t+\tau) c_i(t)\rangle}{\langle c_i^\dagger(t) c_i(t)\rangle \langle c_i^\dagger(t+\tau) c_i(t+\tau)\rangle}, \tag{28}$$

where τ is the time-delay between two measurements. At $\tau = 0$, the second-order correlation function of the three output ports can be expressed as

$$g_{21}(0) = N_1^{-2}\langle a_1^\dagger a_1^\dagger a_1 a_1\rangle, \tag{29a}$$

$$g_{22}(0) = N_2^{-2}\langle a_2^\dagger a_2^\dagger a_2 a_2\rangle, \tag{29b}$$

$$g_{23}(0) = \frac{1}{9N_3^2}\sum_{j,k,m,l=1,2}\sqrt{\gamma_i\gamma_k\gamma_m\gamma_l}\langle a_j^\dagger a_k^\dagger a_m a_l\rangle. \tag{29c}$$

Several previous studies on photon (phonon) blockade equate the concepts of photon antibunching and sub-Poissonian photon-number statistics. However, we treat these effects distinctly according to their standard definitions. Specifically, for stationary fields, photon antibunching (bunching) means that $g_{2i}(\tau) > g_{2i}(0)$ [$g_{2i}(\tau) < g_{2i}(0)$], that is, a local minimum (maximum) around the zero-time delay [94, 97]. The sub-Poissonian (super-Poissonian) photon statistics only indicate that $g_{2i}(0) < 1$ [$g_{2i}(0) > 1$]. Thus, sub-Poissonian statistics does not imply photon antibunching and vice versa [98]. Note that both photon antibunching and sub-Poissonian statistics are key features for an ideal single-photon source. We will show that both of these two purely nonclassical effects can be observed in our proposal.

As discussed in Sec. III.A, given that only states $|00\rangle$, $|10\rangle$, and $|01\rangle$ are of large probabilities, while the two-photon states $|20\rangle$, $|02\rangle$, and $|11\rangle$ are of extremely low probabilities, we will observe single-photon blockade in two resonators: A single photon in one resonator cannot only blockade the second photon in this resonator, but can also blockade another photon from being excited in another resonator. Consequently, once the photon escapes from the two resonators can the system be reexcited. As a result, the photon distribution from ports 1 and 2 are both sub-Poissonian, and the cross-correlation between two resonators displays the anticorrelation. Moreover, in the following sections, we will show that the field from port 3 also exhibits both sub-Poissonian statistics and antibunching. Thus, a single photon can be emitted from ports 1 and 2, or alternatively from port 3.

In Fig. 6, the time-delay second-order correlation functions $g_{2i}(\tau)$ of the steady state of the output port i are plotted, from which we find that $g_{2i}(\tau) \ll 1$ and all show dips at $\tau = 0$, indicating that the output microwave fields from the three ports exhibit both sub-Poissonian photon-number statistics and photon antibunching.

In Fig. 7, we plot the computed values of $\log_{10}[g_{2i}(0)]$ and N_i changing with θ and Δ_+. Here we assume that the drives for the two resonators are of the same strength, while the phase difference between the two microwave drives is θ, i.e, $\epsilon_1 = \epsilon_2^* = \exp(i\theta/2)$, and the corresponding driving strengths for the supermodes A_+ and A_- are $\epsilon_+ = 2\cos(\theta/2)$ and $\epsilon_- = 2i\sin(\theta/2)$, respectively. It is obvious that ϵ_+ (ϵ_-) decreases (increases) with increasing $|\theta|$ in the regime $[0, \pi]$. Since the resonators 1 and 2 are identical, the modes a_1 and a_2 share the same dynamics and, thus, we only plot $g_{21}(0)$ and N_1. In particular, due to $\gamma_1/\gamma_2 = \beta = 1$, for port 3 we have

$$N_3 \propto \langle A_+^\dagger A_+\rangle,$$
$$g_{23}(0) \propto \langle A_+^\dagger A_+^\dagger A_+ A_+\rangle / \langle A_+^\dagger A_+\rangle^2,$$

so the photon statistics of the output field from port 3 is determined only by the properties of the supermode A_+ under these conditions.

In the left panel of Fig. 7, we consider that the two supermodes are degenerate with $\Delta_2 = 0$. Around $\Delta_+ = 0$ (i.e., the drive for the supermode A_+ is resonant), both $g_{21}(0)$ and $g_{23}(0)$ show a dip at $\theta = 0$. However, with increasing $|\theta|$, the driving strength ϵ_- for the supermode A_- goes up, leading to its eigenstates $|\psi_{i-}\rangle$ being effectively excited. It can easily be verified that mode a_1 satisfies

$$\langle \psi_{i-}| a_1^\dagger a_1 |\psi_{i-}\rangle \neq 0, \tag{30a}$$

$$\langle \psi_{j-}| a_1^\dagger a_1^\dagger a_1 a_1 |\psi_{j-}\rangle \neq 0, \tag{30b}$$

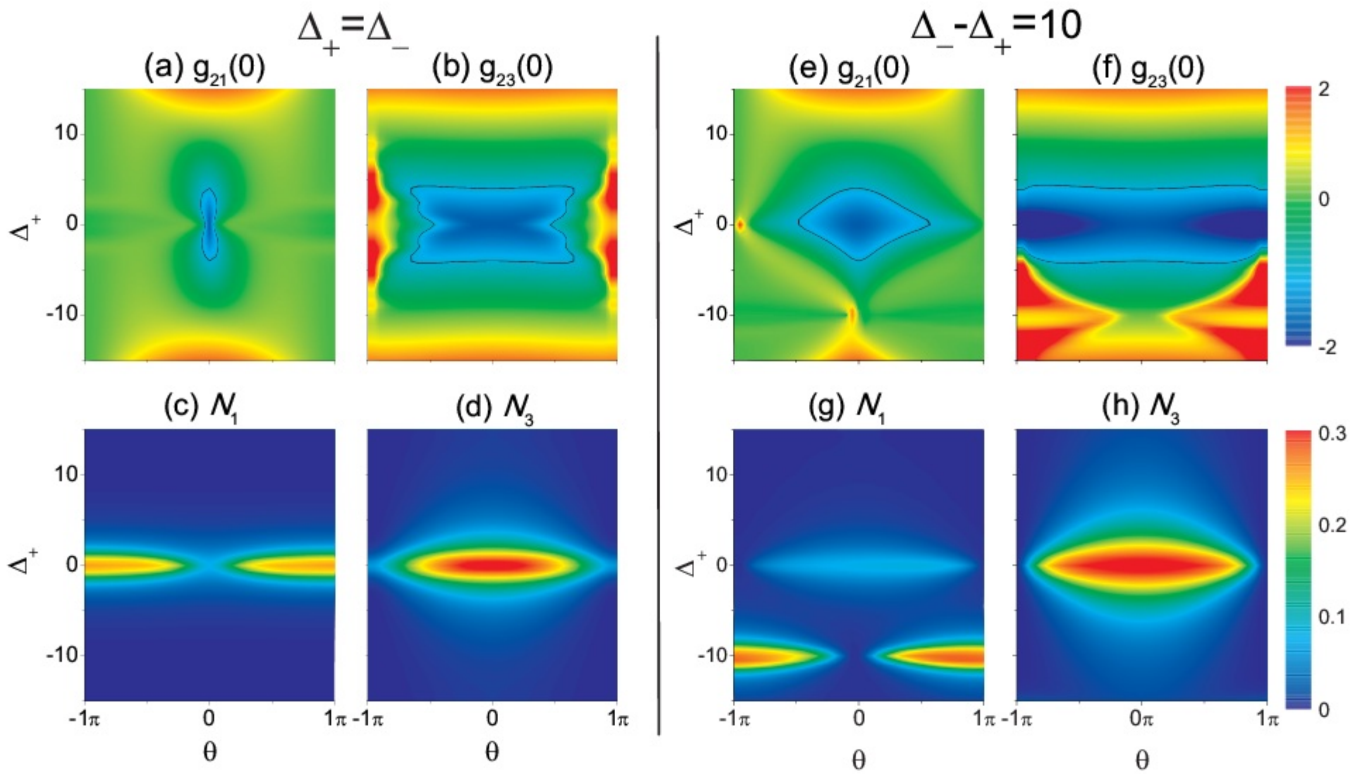

FIG. 7. (Color online) The average photon escape rate N_1 (N_3) and the second-order correlation function $g_{21}(0)$ [$g_{23}(0)$] from port 1 (port 3) versus the drive detuning Δ_+ and the phase difference θ. The left panel corresponds to the degenerate case ($\Delta_2 = 0$) while the right panel shows the nondegenerate case ($\Delta_2 = 10$). Experiments could adjust the coupling capacity C between the two resonators, to change the frequency separation between the two supermodes. In the plot of the second-order correlation function $g_{2i}(0)$, the solid black closed loops in (a, b, e, f) correspond to $\log_{10}[g_{2i}(0)] = -1$ and the points inside the loops indicate that the output fields exhibit a strong sub-Poissonian character. It can be found that, in both degenerate and nondegenerate cases, $g_{21}(0)$ and $g_{23}(0)$ can display dips around $\Delta_+ = 0$ and $\theta = 0$. The other parameters used here are the same as those in Fig. 3(b).

while for supermode A_+:

$$\langle\psi_{i-}|A_+^\dagger A_+|\psi_{i-}\rangle = 0, \tag{31a}$$

$$\langle\psi_{j-}|A_+^\dagger A_+^\dagger A_+ A_+|\psi_{j-}\rangle = 0, \tag{31b}$$

where $i \geq 1$ and $j \geq 2$. Thus, the eigenstates of the supermode A_- being effectively excited lead to the increase of both output photon number N_1 and second-order correlation function $g_{21}(0)$. However, their contributions to N_3 and $g_{23}(0)$ vanish according to Eqs. (31a) and (31b). In Figs. 7(a) and 7(b), it can be found that, compared with $g_{23}(0)$, $g_{21}(0)$ is much more sensitive to the changes of θ: even though θ is a slightly bias from 0, the photon statistics of the output field from port 1 will not be sub-Poissonian any more. In Fig. 7(c) we find that, around $\Delta_+ = 0$, the average photon number N_1 from port 1 increases with $|\theta|$. At $\theta = \pm\pi$, the drive strength for the supermode A_- and the photon number in resonator 1 both reach their maxima. However, the field from port 1 is not sub-Poissonian any more. The photon output N_3 from outport 3 vanishes at $\theta = \pm\pi$, as shown in Fig. 7(d), for two reasons: first, the drive strength ϵ_+ for the supermode A_+ decreases to zero; second, there is no contribution from the eigenstates $|\psi_{j-}\rangle$ of the supermode A_-.

In the right panel of Fig. 7, we plot the non-degenerate case with $\Delta_- - \Delta_+ = 10$. By comparing with the degenerate case, we find that both $g_{21}(0)$ and $g_{23}(0)$ display the sub-Poissonian behavior in a wider range of θ. In this case, despite of increasing θ, the driving strength ϵ_- for the supermode A_- is still far off-resonance around $\Delta_+ = 0$, as shown in Fig. 2. Therefore, the states $|\psi_{i-}\rangle$ cannot be effectively excited, so their contributions for the mode a_1 are negligible. Only the driving ϵ_+ for the supermode A_+ affects N_1 and $g_{21}(0)$. Due to the nonlinear coupling between the supermode A_+ and the qubit, only the state $|\psi_{1+}\rangle$ can be excited effectively. Compared with the degenerate case in Fig. 7(a), $g_{21}(0)$ in Fig. 7(e) is less sensitive to the phase difference θ. In Fig. 7(g), we find that, around $\Delta_+ = -10$, the photon number N_1 from port 1 is very large, owing to the resonant driving of the supermode A_-. Since there is no nonlinear coupling between the supermode A_- and the qubit, multi-photon states for the supermode A_- are excited. Although the output photon number N_1 is large, the second-order correlation function $g_{21}(0)$ is not sub-Poissonian.

Last, we want to discuss another interesting phenomenon. Specifically, if the direct coupling g between the two resonators vanishes (i.e., the capacitor C is removed), the two supermodes A_+ and A_- are still nondegenerate, and the frequency difference is only determined by the dispersive coupling strength, as shown in Eq. (15), i.e, $\Delta_2 = 4G_x^2/(3\Omega_+)$. In this case, even when only one resonator is under a resonantly-coherent drive (for example, $\epsilon_1 = 1$ and $\epsilon_2 = 0$), the phenomenon, that single photon outputs from ports 1, 2, and 3, still exists under the condition

$$\Delta_2 = 4G_x^2/(3\Omega_+) \gg \epsilon_-, \tag{32}$$

which can easily be realized in experiments. Thus, by employing only one coherent drive, and one auxiliary qubit without any direct coupling between two resonators, the single-photon outputs also exist in all the three output channels.

D. Entanglement relation between the two cavities

To analyze the entanglement between the resonators, we use the logarithmic negativity to measure the entanglement, which is given by [99]

$$E_c = \log_2 [N_E(\hat{\rho}_{12}) + 1], \tag{33}$$

where the negativity $N_E(\hat{\rho}_{12})$ quantifies the entanglement of the two-resonator steady state ρ_{12}, which can be expressed as

$$N_E(\hat{\rho}_{12}) = \frac{||\hat{\rho}_{12}^{T_1}|| - 1}{2}. \tag{34}$$

Here T_1 denotes the partial transpose of the density matrix $\hat{\rho}_{12}$ with respect to the resonator 1, and $||\hat{\rho}_{12}^{T_1}||$ is the trace norm of $\hat{\rho}_{12}^{T_1}$. The logarithmic negativity E_c is an entanglement monotone, which can be used for quantifying the entanglement between the two resonators (i.e., the entanglement between signals from ports 1 and 2). In Fig. 8, we adopt the parameters with $\theta = 0$ and $\Delta_2 = 10$, and plot the dependence of E_c on the ratio β. In this case, only the first excited state $|\psi_{1+}\rangle$ of the supermode A_+ can be effectively driven. Note that $|\psi_{1+}\rangle$ is a maximally-entangled state (i.e., the 'triplet' state) when $\beta = 1$. As shown in Fig. 8, we find that the output fields from ports 1 and 2 are entangled, and the logarithmic negativity E_c reaches its maximum value when $\beta = 1$. We find that, the entanglement between fields from these two ports has a close relation with the single-photon blockade effects, which originates from optical state truncation (or the nonlinear quantum scissors). That is, the states of the two cavities are truncated to a qubit, with the single-photon Bell 'triplet' state $|\psi_{1+}\rangle$ being the first-excited state.

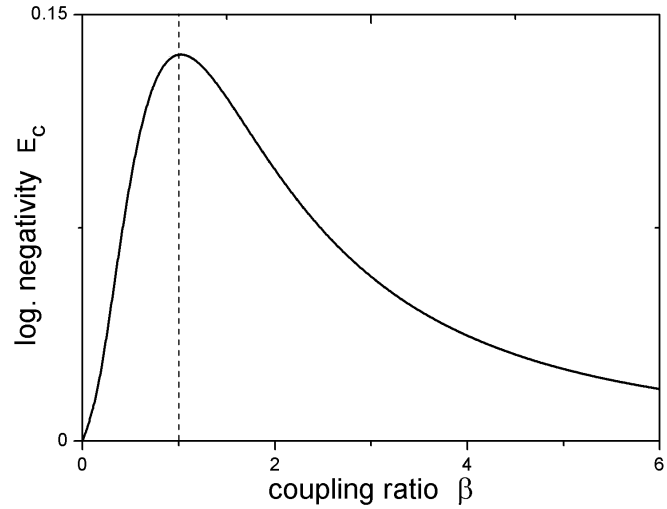

FIG. 8. The logarithmic negativity E_c versus the coupling ratio β. Here we fix $\theta = 0$ and $\Delta_+ = 0$, and other parameters are the same as those of the nondegenerate case in Fig. 7. The vertical dashed line is at $\beta = 1$.

V. DISCUSSION AND CONCLUSIONS

In this paper we demonstrated that it is possible to achieve single-photon outputs in a circuit-QED system based on *both* longitudinal and transverse couplings. We obtained the effective Hamiltonians and the rates for multi-photon processes, and found that the effective nonlinear coupling between one of the supermodes and the qubit can lead to photon blockade effects.

We note the multi-photon processes can also be induced in the hybrid superconducting system with only longitudinal coupling, which has been shown in our previous study [100]. In this work, we found that the second-order nonlinearity can be about one order of magnitude stronger. Moreover, the drive for the qubit is not needed in the present case.

We have analyzed photon blockade in phase space by applying the Cahill-Glauber s-parametrized QPDs. This approach enabled us to show not only the nonclassical character of the states generated via photon blockade, but also to determine the degree of nonclassicality of the states, using the Lee nonclassical depth.

Moreover, we considered two different output channels for the fields: those from the individual resonators and the joint channels of both resonators. It was found that all the three output fields display photon antibunching and sub-Poissonian photon-number distribution. Thus, our proposal can be used to work as multi-output single microwave photon devices. Afterwards, by analyzing the steady-state solutions, we discussed the degenerate and nondegenerate cases of the two supermodes. In the degenerate case, the second-order correlation function $g_{21}(0)$ of port 1 is much more sensitive to the increase of the drive strength ϵ_- for the supermode A_- than in the nondegenerate case. For the joint output 3, due to no contribution from the eigenstates of the supermode A_-, $g_{23}(0)$ is more robust against the increase of ϵ_- than that of $g_{21}(0)$ in both degenerate and nondegenerate cases. We also found that the state truncation of two-resonator modes will lead to the entanglement between two resonators.

Compared with the dispersive and resonant microwave-photon blockade known from previous studies, our proposal has the following two advantages: first, the excited state of the system still retains a photonic nature (i.e., this is a pure single-photon Fock state rather than a polariton state); second, the strong nonlinearity makes it possible to increase the single-photon output rate.

It should be stressed that, to obtain multi-output channels, we consider two resonators in this paper, but these results can also be applied to the simple *single-resonator case*. We believe that our proposal can be helpful in designing single-photon sources in the microwave regime.

ACKNOWLEDGMENTS

The authors acknowledge fruitful discussions with Anton F. Kockum, Wei Qin, Salvatore Savasta, Chui-Ping Yang, and Zhi-Rong Zhong. XW is supported by the China Scholarship Council (Grant No. 201506280142). AM and FN acknowledge the support of a grant from the John Templeton Foundation. FN was also partially supported by the RIKEN iTHES Project, the MURI Center for Dynamic Magneto-Optics via the AFOSR award number FA9550-14-1-0040, the IMPACT program of JST, and a Grant-in-Aid for Scientific Research (A).

[1] A. Kiraz, M. Atatüre, and A. Imamoğlu, "Quantum-dot single-photon sources: Prospects for applications in linear optics quantum-information processing," Phys. Rev. A **69**, 032305 (2004).
[2] H. J. Kimble, "The quantum internet," Nature (London) **453**, 1023 (2008).
[3] J. L. O'Brien, A. Furusawa, and J. Vučković, "Photonic quantum technologies," Nat. Photon. **3**, 687 (2009).
[4] A. Faraon, I. Fushman, D. Englund, N. Stoltz, P. Petroff, and J. Vučković, "Coherent generation of non-classical light on a chip via photon-induced tunnelling and blockade," Nat. Phys. **4**, 859 (2008).
[5] Y. M. He, Y. He, Y. J. Wei, D. Wu, M. Atatüre, C. Schneider, S. Höfling, M. Kamp, C. Y. Lu, and J. W. Pan, "On-demand semiconductor single-photon source with near-unity indistinguishability," Nat. Nanotech. **8**, 213 (2013).
[6] D. F. Walls and G. J. Milburn, *Quantum Optics* (Springer, Berlin, 2007).
[7] V. Scarani, H. Bechmann-Pasquinucci, N. J. Cerf, M. Dušek, N. Lütkenhaus, and M. Peev, "The security of practical quantum key distribution," Rev. Mod. Phys. **81**, 1301 (2009).
[8] L. Tian and H. J. Carmichael, "Quantum trajectory simulations of two-state behavior in an optical cavity containing one atom," Phys. Rev. A **46**, R6801 (1992).
[9] W. Leoński and R. Tanaś, "Possibility of producing the one-photon state in a kicked cavity with a nonlinear Kerr medium," Phys. Rev. A **49**, R20 (1994).
[10] A. Miranowicz, W. Leoński, S. Dyrting, and R. Tanaś, "Quantum state engineering in finite-dimensional Hilbert space," Acta Phys. Slov. **46**, 451 (1996).
[11] A. Imamoğlu, H. Schmidt, G. Woods, and M. Deutsch, "Strongly interacting photons in a nonlinear cavity," Phys. Rev. Lett. **79**, 1467 (1997).
[12] A. Verger, C. Ciuti, and I. Carusotto, "Polariton quantum blockade in a photonic dot," Phys. Rev. B **73**, 193306 (2006).
[13] A. Miranowicz, M. Paprzycka, Y. X. Liu, J. Bajer, and F. Nori, "Two-photon and three-photon blockades in driven nonlinear systems," Phys. Rev. A **87**, 023809 (2013).
[14] A. Majumdar and D. Gerace, "Single-photon blockade in doubly resonant nanocavities with second-order nonlinearity," Phys. Rev. B **87**, 235319 (2013).
[15] Y. X. Liu, X. W. Xu, A. Miranowicz, and F. Nori, "From blockade to transparency: Controllable photon transmission through a circuit-QED system," Phys. Rev. A **89**, 043818 (2014).
[16] X. W. Xu and Y. Li, "Tunable photon statistics in weakly nonlinear photonic molecules," Phys. Rev. A **90**, 043822 (2014).
[17] K. M. Birnbaum, A. Boca, R. Miller, A. D. Boozer, T. E. Northup, and H. J. Kimble, "Photon blockade in an optical cavity with one trapped atom," Nature (London) **436**, 87 (2005).
[18] A. Faraon, A. Majumdar, D. Englund, E. Kim, M. Bajcsy, and J. Vučković, "Integrated quantum optical networks based on quantum dots and photonic crystals," New J. Phys. **13**, 055025 (2011).
[19] A. Majumdar, M. Bajcsy, and J. Vučković, "Probing the ladder of dressed states and nonclassical light generation in quantum-dot–cavity QED," Phys. Rev. A **85**, 041801 (2012).
[20] A. J. Hoffman, S. J. Srinivasan, S. Schmidt, L. Spietz, J. Aumentado, H. E. Türeci, and A. A. Houck, "Dispersive photon blockade in a superconducting circuit," Phys. Rev. Lett. **107**, 053602 (2011).
[21] C. Lang, D. Bozyigit, C. Eichler, L. Steffen, J. M. Fink, A. A. Abdumalikov, M. Baur, S. Filipp, M. P. da Silva, A. Blais, and A. Wallraff, "Observation of resonant photon blockade at microwave frequencies using correlation function measurements," Phys. Rev. Lett. **106**, 243601 (2011).
[22] Y.-X. Liu, A. Miranowicz, Y. B. Gao, J. Bajer, C. P. Sun, and F. Nori, "Qubit-induced phonon blockade as a signature of quantum behavior in nanomechanical resonators," Phys. Rev. A **82**, 032101 (2010).
[23] N. Didier, S. Pugnetti, Y. M. Blanter, and R. Fazio, "Detecting phonon blockade with photons," Phys. Rev. B **84**, 054503 (2011).

[24] P. Rabl, "Photon blockade effect in optomechanical systems," Phys. Rev. Lett. **107**, 063601 (2011).

[25] J. Q. Liao and F. Nori, "Photon blockade in quadratically coupled optomechanical systems," Phys. Rev. A **88**, 023853 (2013).

[26] X. W. Xu, Y. J. Li, and Y. X. Liu, "Photon-induced tunneling in optomechanical systems," Phys. Rev. A **87**, 025803 (2013).

[27] H. Wang, X. Gu, Y. X. Liu, A. Miranowicz, and F. Nori, "Tunable photon blockade in a hybrid system consisting of an optomechanical device coupled to a two-level system," Phys. Rev. A **92**, 033806 (2015).

[28] A. Miranowicz and W. Leoński, "Two-mode optical state truncation and generation of maximally entangled states in pumped nonlinear couplers," J. Phys. B **39**, 1683 (2006).

[29] T. C. H. Liew and V. Savona, "Single photons from coupled quantum modes," Phys. Rev. Lett. **104**, 183601 (2010).

[30] R. Stassi, S. De Liberato, L. Garziano, B. Spagnolo, and S. Savasta, "Quantum control and long-range quantum correlations in dynamical Casimir arrays," Phys. Rev. A **92**, 013830 (2015).

[31] M. Bamba, A. Imamoğlu, I. Carusotto, and C. Ciuti, "Origin of strong photon antibunching in weakly nonlinear photonic molecules," Phys. Rev. A **83**, 021802 (2011).

[32] S. Ferretti, V. Savona, and D. Gerace, "Optimal antibunching in passive photonic devices based on coupled nonlinear resonators," New J. Phys. **15**, 025012 (2013).

[33] M. A. Lemonde, N. Didier, and A. A. Clerk, "Antibunching and unconventional photon blockade with Gaussian squeezed states," Phys. Rev. A **90**, 063824 (2014).

[34] O. Kyriienko, I. A. Shelykh, and T. C. H. Liew, "Tunable single-photon emission from dipolaritons," Phys. Rev. A **90**, 033807 (2014).

[35] Y. H. Zhou, H. Z. Shen, and X. X. Yi, "Unconventional photon blockade with second-order nonlinearity," Phys. Rev. A **92**, 023838 (2015).

[36] J. Tang, W. D. Geng, and X. L. Xu, "Quantum interference induced photon blockade in a coupled single quantum dot-cavity system," Sci. Rep. **5**, 9252 (2015).

[37] G. H. Hovsepyan, A. R. Shahinyan, and G. Yu. Kryuchkyan, "Multiphoton blockades in pulsed regimes beyond stationary limits," Phys. Rev. A **90**, 013839 (2014).

[38] A. Miranowicz, J. Bajer, M. Paprzycka, Y. X. Liu, A. M. Zagoskin, and F. Nori, "State-dependent photon blockade via quantum-reservoir engineering," Phys. Rev. A **90**, 033831 (2014).

[39] A. Miranowicz, M. Paprzycka, A. Pathak, and F. Nori, "Phase-space interference of states optically truncated by quantum scissors: Generation of distinct superpositions of qudit coherent states by displacement of vacuum," Phys. Rev. A **89**, 033812 (2014).

[40] A. Miranowicz, J. Bajer, N. Lambert, Y. X. Liu, and F. Nori, "Tunable multiphonon blockade in coupled nanomechanical resonators," Phys. Rev. A **93**, 013808 (2016).

[41] I. I. Smolyaninov, A. V. Zayats, A. Gungor, and C. C. Davis, "Single-photon tunneling via localized surface plasmons," Phys. Rev. Lett. **88**, 187402 (2002).

[42] I. Schuster, A. Kubanek, A. Fuhrmanek, T. Puppe, P. W. H. Pinkse, K. Murr, and G. Rempe, "Nonlinear spectroscopy of photons bound to one atom," Nat. Phys. **4**, 382 (2008).

[43] A. Kubanek, A. Ourjoumtsev, I. Schuster, M. Koch, P. W. H. Pinkse, K. Murr, and G. Rempe, "Two-photon gateway in one-atom cavity quantum electrodynamics," Phys. Rev. Lett. **101**, 203602 (2008).

[44] A. Miranowicz, W. Leoński, and N. Imoto, "Quantum-optical states in finite-dimensional Hilbert space. i. general formalism," Adv. Chem. Phys. **119(I)**, 155 (2001).

[45] W. Leoński and A. Miranowicz, "Quantum-optical states in finite-dimensional Hilbert space. ii. state generation," Adv. Chem. Phys. **119(I)**, 195 (2001).

[46] J. Q. You and F. Nori, "Superconducting circuits and quantum information," Phys. Today **58**, 42 (2005).

[47] I. Buluta, S. Ashhab, and F. Nori, "Natural and artificial atoms for quantum computation," Rep. Prog. Phys. **74**, 104401 (2011).

[48] J. Q. You and F. Nori, "Atomic physics and quantum optics using superconducting circuits," Nature (London) **474**, 589 (2011).

[49] Z. L. Xiang, S. Ashhab, J. Q. You, and F. Nori, "Hybrid quantum circuits: Superconducting circuits interacting with other quantum systems," Rev. Mod. Phys. **85**, 623 (2013).

[50] L. DiCarlo, M. D. Reed, L. Sun, B. R. Johnson, J. M. Chow, J. M. Gambetta, L. Frunzio, S. M. Girvin, M. H. Devoret, and R. J. Schoelkopf, "Preparation and measurement of three-qubit entanglement in a superconducting circuit," Nature (London) **467**, 574 (2010).

[51] E. Lucero, R. Barends, Y. Chen, J. Kelly, M. Mariantoni, A. Megrant, P. OMalley, D. Sank, A. Vainsencher, J. Wenner, Y. Yin, A. N. Cleland, and J. M. Martinis, "Computing prime factors with a Josephson phase qubit quantum processor," Nat. Phys. **8**, 719 (2012).

[52] G. Romero, J. J. García-Ripoll, and E. Solano, "Microwave photon detector in circuit QED," Phys. Rev. Lett. **102**, 173602 (2009).

[53] B. Peropadre, G. Romero, G. Johansson, C. M. Wilson, E. Solano, and J. J. García-Ripoll, "Approaching perfect microwave photodetection in circuit QED," Phys. Rev. A **84**, 063834 (2011).

[54] Y. F. Chen, D. Hover, S. Sendelbach, L. Maurer, S. T. Merkel, E. J. Pritchett, F. K. Wilhelm, and R. McDermott, "Microwave photon counter based on Josephson junctions," Phys. Rev. Lett. **107**, 217401 (2011).

[55] **093601** (2014).

[56] K. Inomata, Z. R. Lin, K. Koshino, W. D. Oliver, J. S. Tsai, T. Yamamoto, and Y. Nakamura, "Single microwave-photon detector using an artificial λ-type three-level system," arXiv:1601.05513 (2016).

[57] C. Lang, C. Eichler, L. Steffen, J. M. Fink, M. J. Woolley, A. Blais, and A. Wallraff, "Correlations, indistinguishability and entanglement in Hong-Ou-Mandel experiments at microwave frequencies," Nat. Phys. **9**, 345 (2013).

[58] S. Virally, J. O. Simoneau, C. Lupien, and B. Reulet, "Discrete photon statistics from continuous microwave measurements," Phys. Rev. A **93**, 043813 (2016).

[59] A. Ridolfo, M. Leib, S. Savasta, and M. J. Hartmann, "Photon blockade in the ultrastrong coupling regime," Phys. Rev. Lett. **109**, 193602 (2012).

[60] F. W. Strauch, K. Jacobs, and R. W. Simmonds, "Arbitrary control of entanglement between two superconducting resonators," Phys. Rev. Lett. **105**, 050501 (2010).

[61] P. B. Li, S. Y. Gao, and F. L. Li, "Engineering two-mode entangled states between two superconducting resonators by dissipation," Phys. Rev. A **86**, 012318 (2012).

[62] Y. J. Zhao, Y. L. Liu, Y. X. Liu, and F. Nori, "Generating nonclassical photon states via longitudinal couplings between superconducting qubits and microwave fields," Phys. Rev. A **91**, 053820 (2015).

[63] L. Garziano, R. Stassi, V. Macrì, A. F. Kockum, S. Savasta, and F. Nori, "Multiphoton quantum Rabi oscillations in ultrastrong cavity QED," Phys. Rev. A **92**, 063830 (2015).

[64] D. L. Underwood, W. E. Shanks, J. Koch, and A. A. Houck, "Low-disorder microwave cavity lattices for quantum simulation with photons," Phys. Rev. A **86**, 023837 (2012).

[65] J. E. Mooij, T. P. Orlando, L. Levitov, L. Tian, C. H. van der Wal, and S. Lloyd, "Josephson persistent-current qubit," Science **285**, 1036 (1999).

[66] J. Q. You, Y. X. Liu, C. P. Sun, and F. Nori, "Persistent single-photon production by tunable on-chip micromaser with a superconducting quantum circuit," Phys. Rev. B **75**, 104516 (2007).

[67] J. Q. You, Y. X. Liu, and F. Nori, "Simultaneous cooling of an artificial atom and its neighboring quantum system," Phys. Rev. Lett. **100**, 047001 (2008).

[68] F. G. Paauw, A. Fedorov, C. J. P. M Harmans, and J. E. Mooij, "Tuning the gap of a superconducting flux qubit," Phys. Rev. Lett. **102**, 090501 (2009).

[69] A. Le Boité, M. J. Hwang, H. Nha, and M. B. Plenio, "Fate of photon blockade in the deep strong-coupling regime," Phys. Rev. A **94**, 033827 (2016).

[70] Y. D. Wang, A. Kemp, and K. Semba, "Coupling superconducting flux qubits at optimal point via dynamic decoupling with the quantum bus," Phys. Rev. B **79**, 024502 (2009).

[71] Y. X. Liu, C. X. Yang, H. C. Sun, and X. B. Wang, "Coexistence of single-and multi-photon processes due to longitudinal couplings between superconducting flux qubits and external fields," New J. Phys. **16**, 015031 (2014).

[72] N. Didier, J. Bourassa, and A. Blais, "Fast quantum nondemolition readout by parametric modulation of longitudinal qubit-oscillator interaction," Phys. Rev. Lett. **115**, 203601 (2015).

[73] X. Wang, H. R. Li, D. X. Chen, W. X. Liu, and F. L. Li, "Tunable electromagnetically induced transparency in a composite superconducting system," Opt. Commun. **366**, 321 (2016).

[74] I. Wilson-Rae, P. Zoller, and A. Imamoğlu, "Laser cooling of a nanomechanical resonator mode to its quantum ground state," Phys. Rev. Lett. **92**, 075507 (2004).

[75] D. Leibfried, R. Blatt, C. Monroe, and D. Wineland, "Quantum dynamics of single trapped ions," Rev. Mod. Phys. **75**, 281 (2003).

[76] I. Chiorescu, P. Bertet, K. Semba, Y. Nakamura, C. J. P. M. Harmans, and J. E. Mooij, "Coherent dynamics of a flux qubit coupled to a harmonic oscillator," Nature (London) **431**, 159 (2004).

[77] J. Johansson, S. Saito, T. Meno, H. Nakano, M. Ueda, K. Semba, and H. Takayanagi, "Vacuum Rabi oscillations in a macroscopic superconducting qubit lc oscillator system," Phys. Rev. Lett. **96**, 127006 (2006).

[78] A. A. Abdumalikov, O. Astafiev, Y. Nakamura, Y. A. Pashkin, and J. S. Tsai, "Vacuum Rabi splitting due to strong coupling of a flux qubit and a coplanar-waveguide resonator," Phys. Rev. B **78**, 180502 (2008).

[79] F. Yoshihara, K. Harrabi, A. O. Niskanen, Y. Nakamura, and J. S. Tsai, "Decoherence of flux qubits due to 1/f flux noise," Phys. Rev. Lett. **97**, 167001 (2006).

[80] A. Megrant, C. Neill, R. Barends, B. Chiaro, Yu Chen, L. Feigl, J. Kelly, E. Lucero, M. Mariantoni, P. J. J. O'Malley, D. Sank, A. Vainsencher, J. Wenner, T. C. White, Y. Yin, J. Zhao, C. J. Palmstrm, J. M. Martinis, and A. N. Cleland, "Planar superconducting resonators with internal quality factors above one million," Appl. Phys. Lett. **100**, 113510 (2012).

[81] S. Puri and A. Blais, "High-fidelity resonator-induced phase gate with single-mode squeezing," Phys. Rev. Lett. **116**, 180501 (2016).

[82] W. Leoński and A. Miranowicz, "Kerr nonlinear coupler and entanglement," J. Opt. B **6**, S37 (2004).

[83] H. Flayac and V. Savona, "Input-output theory of the unconventional photon blockade," Phys. Rev. A **88**, 033836 (2013).

[84] M. J. Collett and C. W. Gardiner, "Squeezing of intracavity and traveling-wave light fields produced in parametric amplification," Phys. Rev. A **30**, 1386 (1984).

[85] C. W. Gardiner and M. J. Collett, "Input and output in damped quantum systems: Quantum stochastic differential equations and the master equation," Phys. Rev. A **31**, 3761 (1985).

[86] J. R. Johansson, P. D. Nation, and F. Nori, "Qutip: An open-source Python framework for the dynamics of open quantum systems," Comput. Phys. Commun. **183**, 1760 (2012).

[87] J. R. Johansson, P. D. Nation, and F. Nori, "Qutip 2: A Python framework for the dynamics of open quantum systems," Comput. Phys. Commun. **184**, 1234 (2013).

[88] A. Kamenev, *The Theory of Open Quantum Systems* (Cambridge University Press, Cambridge, 2011).

[89] M.-A. Lemonde, N. Didier, and A. A. Clerk, "Enhanced nonlinear interactions in quantum optomechanics via mechanical amplification," Nat. Commun. **7**, 11338 (2016).

[90] H. P. Breuer and F. Petruccione, *The Theory of Open Quantum Systems* (Oxford University Press, Oxford, 2003).

[91] F. Beaudoin, J. M. Gambetta, and A. Blais, "Dissipation and ultrastrong coupling in circuit QED," Phys. Rev. A **84**, 043832 (2011).

[92] K. E. Cahill and R. J. Glauber, "Ordered expansions in boson amplitude operators," Phys. Rev. **177**, 1857 (1969).

[93] J. Spanier and K. B. Oldham, *An Atlas of Functions* (Hemisphere, Washington/Springer, Berlin, 1995).

[94] A. Miranowicz, M. Bartkowiak, X. G. Wang, Y. X. Liu, and F. Nori, "Testing nonclassicality in multimode fields: A unified derivation of classical inequalities," Phys. Rev. A **82**, 013824 (2010).

[95] A. Miranowicz, K. Bartkiewicz, A. Pathak, J. Peřina Jr, Y. N. Chen, and F. Nori, "Statistical mixtures of states can be more quantum than their superpositions:

Comparison of nonclassicality measures for single-qubit states," Phys. Rev. A **91**, 042309 (2015).

[96] C. T. Lee, "Measure of the nonclassicality of nonclassical states," Phys. Rev. A **44**, R2775 (1991).

[97] L. Mandel and E. Wolf, *Optical Coherence and Quantum Optics* (Cambridge University Press, Cambridge, 1995).

[98] X. T. Zou and L. Mandel, "Photon-antibunching and sub-Poissonian photon statistics," Phys. Rev. A **41**, 475 (1990).

[99] R. Horodecki, P. Horodecki, M. Horodecki, and K. Horodecki, "Quantum entanglement," Rev. Mod. Phys. **81**, 865–942 (2009).

[100] X. Wang, A. Miranowicz, H. R. Li, and F. Nori, "Method for observing robust and tunable phonon blockade in a nanomechanical resonator coupled to a charge qubit," Phys. Rev. A **93**, 063861 (2016).